PPPL--2676

DE90 008152

Image reconstruction methods for the PBX-M pinhole camera

A. Holland, E. T. Powell, and R. J. Fonck
Princeton Plasma Physics Laboratory, Princeton University
P.O. Box 451, Princeton, NJ 08543

This paper describes two methods which have been used to reconstruct the soft X-ray emission profile of the PBX-M tokamak from the projected images recorded by the PBX-M pinhole camera.[1] Both methods must accurately represent the shape of the reconstructed profile while also providing a degree of immunity to noise in the data.

The first method is a simple least squares fit to the data. This has the advantage of being fast and small, and thus easily implemented on the PDP-11 computer used to control the video digitizer for the pinhole camera.

The second method involves the application of a maximum entropy algorithm to an overdetermined system. This has the advantage of allowing the use of a default profile. This profile contains additional knowledge about the plasma shape which can be obtained from equilibrium fits to the external magnetic measurements. Additionally the reconstruction is guaranteed positive, and the fit to the data can be relaxed by specifying both the amount and distribution of noise in the image. The algorithm described has the advantage of being considerably faster, for an overdetermined system, than the usual Lagrange multiplier approach[2,3] to finding the maximum entropy solution.

MASTER

DISTRIBUTION OF THIS DOCUMENT IS UNLIMITED

I. Introduction

The PBX-M pinhole camera provides a toroidally integrated view from a point on the outer midplane of the PBX-M plasma, as shown in Fig. 1 . The X-ray emission profile is generally a bean-shaped toroid and the goal of the reconstruction procedure is to obtain the emission profile over a poloidal section through the toroid. For this application the features of interest are the shapes of the contours of constant X-ray emission since they can then be used to infer the internal magnetic properties of the plasma.[4]

A. General features of both reconstruction methods

1. The emission profile is assumed to be toroidally symmetric.
2. The camera supplies a 128 × 128 pixel image which is reduced to a 32 × 32 image of 1024 pixels for the subsequent analysis.
3. Each pixel samples the emission from a volume of plasma which is determined simply by the projection of the pixel through a pinhole aperture.

The nature of the projection provided by this geometry is such that the the number of pixels sampling a toroidal ring of plasma with a small cross section increases greatly as the center of the ring's cross section is moved closer to the midplane and closer to the outer edge of the plasma. Fig. 2 shows contours of the function specifying total contribution of each region in a poloidal section of the plasma to the projected image. This means that the reconstructed emission profile is very well determined near the outer midplane and is progressively more sensitive to noise in the data in regions which are further from the midplane and closer to the center of the torus.

B. Formulation of the problem

The emission profile is specified as a set of $\{E_c\}$ values assigned to NC toroidal rings with a rectangular cross section. Each value E_c is the emission per unit volume of the source averaged over ring c. In order to provide good shape resolution near the center of the plasma while maintaining an

acceptably low sensitivity to noise in the data, the emission profile is specified on a dual resolution grid which has smaller cells in the outer midplane region. In addition, cells which are in regions with no plasma or cells which are hidden from view are eliminated. This results in the bean-shaped grid shown in Fig. 3 which shows a poloidal section through a grid of 130 rings.

The emission values $\{E_c\}$ are mapped linearly onto the NP pixels of the camera image $\{I_p\}$ by the usual imaging equations

$$I_p = \sum_{c=1}^{NC} S_{pc} E_c + n_p. \tag{1}$$

The elements S_{pc} of the $NP \times NC$ matrix $\mathbf{S}$ are computed from the geometry of the system and represent the sensitivity of pixel p to the emission from cell c. The values $\{n_p\}$ represent the noise in the data.

II. Least squares method

Since the problem has been formulated as an overdetermined system with 1023 image pixels and only 130 emission cells, the emission profile can be recovered by a simple least squares fit[5] which minimizes $\sum n_p^2$. The emission vector $\mathbf{E}$ is computed from the image vector $\mathbf{I}$ by multiplication by the generalized inverse of $\mathbf{S}$.

$$\mathbf{E} = (\mathbf{S^T S})^{-1} \mathbf{S^T I} = \mathbf{M I}.$$

The inverse matrix $\mathbf{M}$ is computed once for a given reconstruction grid and camera geometry and then saved for repeated use. Since computing the emission profile for each image just involves multiplying a matrix by a vector, the algorithm can easily be implemented and is relatively fast.

A. Negative values

The most obvious problem with the method is that it allows solutions with negative values for the emissions $\{E_c\}$. Negative values are caused by noise in the data or numerical errors in the matrix inversion and multiplication. Since they usually occur in cells near regions in the original source with small

or zero emission, we remove them from the final solution by assigning them to zero or to a small percentage of the average emission of the solution.

B. Smoothing

We also tested the effect of applying smoothing to the reconstructed emission profile obtained from the least squares method. The smoothing procedure is described as follows.

1. Obtain the emission at any point $E(r, Z)$ from the reconstructed $\{E_c\}$ using bilinear interpolation from the centers of the surrounding cells.
2. Compute the average value $E(r, Z)$ for each cell.
3. Set the emissions $\{E_c\}$ equal to the average values from step 2.

The effect of this procedure is to apply a longer scale length smoothing in regions of the grid containing larger cells. Stronger smoothing is obtained by applying the procedure several times.

C. Tests

Test data were constructed by specifying a set of emissions $\{E_c\}$ which describe a suitable test source and then computing the corresponding image $\{I_p\}$ using Eqs. (1). The noise values $\{n_p\}$ were simulated using a Gaussian random noise generator. A global estimate of the accuracy is the RMS deviation from the original source defined as

$$\Delta_{rms} = \frac{100}{\overline{E}^{\,reconstructed}} \times \sum_{c=1}^{NC} \left(E_c^{reconstructed} - E_c^{original} \right)^2 \quad \%,$$

where $\overline{E}^{\,reconstructed}$ is the average reconstructed emission.

The result is shown in Fig. 4 for noise with a standard deviation equal to 10% of the average signal applied to each signal value. The original source is shown in Fig. 5 and the cell grid is shown in Fig. 3. Smoothing can improve the appearance and RMS deviation at the expense of spatial resolution as shown in Fig. 6.

Even though the system is 8[$\approx$ (1024 *image pixels*)/(130 *cells*)] times overdetermined, it is still quite sensitive to noise. It is possible to obtain a better result by giving up spatial resolution in less overdetermined regions of the source beforehand by using a more overdetermined cell grid shown in Fig. 7. This grid, which contains 76 cells, is 13.5 times overdetermined. The result for the same noise and source is shown in Fig. 8.

D. Effect of smoothing

Although smoothing improves the RMS deviation and appearance of the result, it does so because the original source is relatively smooth. The smoothing procedure is rather arbitrary since it does not take into account the original imaging Eqs. (1) for the system. During smoothing the noise for each signal n_p can assume any value, and the emission assigned to a cell does not depend on the constraints imposed by the imaging equations. No account is taken of how overdetermined the value of a particular cell may be except for the fact that a shorter scale length smoothing is applied in the higher resolution parts of the grid.

The maximum entropy method described next guarantees a positive definite solution and also allows for smoothing, which is consistent with the imaging equations and the statistics of the noise values $\{n_p\}$.

III. Maximum entropy method

A. Introduction

As shown by Frieden[6] the maximum entropy method is a maximum likelihood estimator derived from the requirement that we select the solution which has maximum probability for given noise and object statistics.

$$P^{object}(\{E_c\})P^{noise}(\{n_p\}|\{E_c\}) = maximum. \tag{2}$$

$P^{noise}(\{n_p\}|\{E_c\})$ is the probability of a given set of noise values $\{n_p\}$, given a particular object $\{E_c\}$. For Gaussian noise statistics

$$P^{noise}(\{n_p\}|\{E_c\}) = \prod_{p=1}^{NP} \frac{1}{\sqrt{2\pi}\sigma_p} \exp\left(-n_p^2/2\sigma_p^2\right),$$

where $\{\sigma_p\}$ are the standard deviations of each signal measurement.

It is usually convenient to maximize the logarithm of Eq. (2). Thus we arrive at the maximum entropy estimator

$$-\sum_{c=1}^{NC} E_c \ln\left(\frac{E_c}{g_c}\right) - \frac{\lambda^2}{2C^2} \sum_{p=1}^{NP} \frac{n_p^2}{\sigma_p^2} = maximum. \tag{3}$$

The values $\{g_c\}$ represent the emission values corresponding to the most probable object. Equation (3) is maximized subject to the constraints implied by the imaging Eqs. (1) and a constraint on the total emission from the system[2,3] which arises in the definition of P^{object}.

$$I_0 = \sum_{c=1}^{NC} E_c. \tag{4}$$

The constant λ^2/C^2, which represents the relative normalization of P^{object} and P^{noise}, is used to set the RMS noise in the final solution. Smaller values of λ^2/C^2 produce solutions with a larger RMS noise. For $\lambda^2/C^2 = 0$ the constraints provided by the imaging equations are relaxed completely and the solution has the profile given by the default image $\{g_c\}$ multiplied by a constant such that the total emission satisfies Eq. (4).

B. Connection to least squares

If $P^{object} = constant$, Eq. (3) reduces to

$$\sum_{p=1}^{NP} \frac{n_p^2}{\sigma_p^2} = minimum$$

which, subject to the constraints of the imaging equations, is just a weighted least squares fit. Thus, least squares is the maximum likelihood estimator when all possible objects (including negative ones) are equally probable.

The method described earlier is an unweighted least squares procedure, but a weighted least squares procedure is easily constructed by dividing each I_p by σ_p and dividing each row S_{pc} by σ_p before calculating the inverse matrix[7] M.

C. Computing the solution

Lagrange multiplier[2,3,8] and less efficient but more easily implemented recursive[9] methods have been used to find the maximum of Eq. (3) subject to the constraints from Eqs. (1) and (4). The same techniques have been used for Poisson noise statistics[8,10] and the conjugate gradient method has been applied for the case of uniform band limited noise with an orthogonal mapping matrix[11,12] S.

1. Lagrange multiplier method

Application of the Lagrange multiplier method produces a solution with one Lagrange multiplier for each constraint equation. The Lagrange multipliers are then computed using an iterative Newton-Raphson method which requires the inversion of a $NL \times NL$ matrix on each iteration where NL is the number of Lagrange multipliers.

This is quite inefficient for an overdetermined system. There are $NC+NP$ free parameters from $\{E_c\}$, $\{n_p\}$, and $NP+1$ constraints from Eqs. (1) and (4) so there are only $NC-1$ degrees of freedom in the maximization; but the Lagrange multiplier technique requires adjustment of $NL > NP > NC$ Lagrange multipliers.

For our application, where $NP = 1024$ and $NC \approx 100 \rightarrow 200$, the method is infeasible on a VAX 8600.

2. Back substitution

As an alternative to the Lagrange multiplier method, we chose to eliminate the constraint Eqs. (1) and (4) from the problem by back substitution. From Eq. (4) we see that the emission from any particular cell can be written

in terms of all the remaining cells. For notational convenience we pick cell 1.

$$E_1 = I_0 - \sum_{c=2}^{NC} E_c \tag{5}$$

The imaging equations can be used to express the noise values $\{n_p\}$ in terms of the measurements $\{I_p\}$ and the cell values $\{E_c\}$. So we now have to do an unconstrained maximization of

$$-E_1 \ln\left(\frac{E_1}{g_1}\right) - \sum_{c=2}^{NC} E_c \ln\left(\frac{E_c}{g_c}\right) - \frac{\lambda^2}{2C^2} \sum_{p=1}^{NP} \frac{(I_p - a_p)^2}{\sigma_p^2}, \tag{6}$$

where a_p is the noise free signal

$$a_p = I_p - n_p = S_{p1}E_1 + \sum_{c=2}^{NC} S_{pc}E_c.$$

To obtain the solution, we set the derivatives of expression (6) with respect to the remaining $NC-1$ values $E_2 \ldots E_{NC}$ equal to zero.

$$F_j = \ln\left(\frac{E_j g_1}{E_1 g_j}\right) - \frac{\lambda^2}{C^2} \sum_{p=1}^{NP} \frac{(I_p - a_p)}{\sigma_p^2}(S_{pj} - S_{p1}) = 0, \quad j = 2 \rightarrow NC. \tag{7}$$

At this point we solve Eqs. (7) iteratively using a Newton-Raphson method[3,13] in $NC-1$ dimensions. We iterate

$$\mathbf{\Delta E} = -\mathbf{D}^{-1}\mathbf{F} \quad where \quad D_{jk} = \frac{\partial F_j}{\partial E_k} \tag{8}$$

and $\mathbf{\Delta E}$ is a vector containing the increments to be applied to $E_2 \ldots E_{NC}$. The elements of $\mathbf{D}$ are given by

$$\frac{\partial F_j}{\partial E_j} = \frac{1}{E_1} + \frac{1}{E_j} + \frac{\lambda^2}{C^2} \sum_{p=1}^{NP} \frac{(S_{pj} - S_{p1})}{\sigma_p^2}, \quad j = 2 \rightarrow NC, \tag{9}$$

and

$$\frac{\partial F_j}{\partial E_k} = \frac{1}{E_1} + \frac{\lambda^2}{C^2} \sum_{p=1}^{NP} \frac{(S_{pj} - S_{p1})(S_{pk} - S_{p1})}{\sigma_p^2}, \quad k \neq j \;\; k, j = 2 \rightarrow NC. \tag{10}$$

Similar expressions for the case of Poisson noise statistics are given in the appendix.

3. Implementation Details

The summations in Eqs. (9) and (10) are constants for a given system and standard deviation profile so the matrix **D** can be quickly loaded if these values are saved prior to beginning the iterations. **D** is a symmetric positive definite matrix which can be inverted using Cholesky decomposition. For an overdetermined system the inversion time for this $(NC - 1) \times (NC - 1)$ matrix is much faster than the $(NP + 1) \times (NP + 1)$ matrix required in the Lagrange multiplier method. For our case the inversion time is $\approx (1025/129)^3$[*i.e.* $\approx$ 500 times] less than the Lagrange multiplier method when using a 130 cell grid. Typically the solution converges in $10 \rightarrow 20$ iterations and takes $30 \rightarrow 60$ seconds on a VAX 8600. The starting point for the iterations is set as follows:

1. The initial values for the $\{E_c\}$ are obtained from the smoothed least squares method described earlier. Any values of $E_c \leq 0$ are removed by setting them to 1% of the average emission.

2. The value for I_0 is taken from the least squares solution. Since I_0 is a global property, the least squares value is usually quite accurate.

3. If the value of $\mathbf{\Delta E}$ from Eq. (8) causes one or more of the E_c to become ≤ 0, the size of $\mathbf{\Delta E}$ is reduced by a factor 2^{Nrelax}, where $Nrelax$ is the smallest power of 2 which will make all the $E_c \geq 0$.

4. The value λ^2/C^2 is initialized and then adjusted periodically during the iterations so that the final solution has a specific total noise requested by the user. The procedure for this is described in the next section.

4. Adjustment of total noise

Since it is generally desirable to control the total amount of noise in the final solution, we introduce a total noise constraint

$$F_{noise} = \sum_{p=1}^{NP} n_p^2 \Big/ \left(\sum_{p=1}^{NP} \sigma_p^2 \right) - 1 = 0. \qquad (11)$$

where C specifies the required total noise as a multiple of the value expected from the standard deviations. The value of λ is adjusted so that Eq. (11) is satisfied.

When solving for the $\{E_c\}$ in the main iterative loop, λ is treated as a constant. If the user picks a value for λ from experience with previous solutions and the total noise in the final solution is within acceptable limits, no further adjustment is necessary. However, if we wish to satisfy Eq. (11) exactly, it is necessary to adjust λ after obtaining a solution for the $\{E_c\}$ and then resolve for the $\{E_c\}$ with the new value of λ. To determine the adjustment to λ, we assume that Eqs. (7) are satisfied and that λ is a nonlinear function of $\{E_c\}$ which has to be adjusted iteratively using the Newton-Raphson method. The required adjustment to λ is given by

$$\Delta\lambda = -F_{noise} \Big/ \left(\frac{\partial F_{noise}}{\partial E_k} \frac{dE_k}{d\lambda} \right), \quad k = 2 \rightarrow NC,$$

where

$$\frac{\partial F_{noise}}{\partial E_k} = -\frac{2}{C^2} \sum_{p=1}^{NP} n_p (S_{pk} - S_{p1}) \Big/ \sum_{p=1}^{NP} \sigma_p^2 ,$$

and we can obtain $dE_k/d\lambda$ from Eqs. (7)

$$\frac{dF_j}{d\lambda} = \frac{\partial F_j}{\partial E_k} \frac{dE_k}{d\lambda} + F_j' = 0$$

where

$$F_j' = -\frac{2\lambda}{C^2} \sum_{p=1}^{NP} \frac{n_p^2}{\sigma_p^2} (S_{pj} - S_{p1}). \tag{12}$$

The terms $\partial F_j / \partial E_k$ are just the elements of $\mathbf{D}$ defined earlier, so

$$\frac{\mathbf{dE}}{\mathbf{d}\lambda} = -\mathbf{D}^{-1}\mathbf{F}'.$$

In practice we do not wait until the $\{E_c\}$ are fully converged and Eqs. (7) are satisfied before making an adjustment to λ. It is normally possible to adjust λ after every $3 \rightarrow 4$ iterations of the main loop without disrupting the convergence to a solution.

To estimate an initial value for λ we take the solution from the smoothed least squares method $\{E_c^{LS}\}$, $\{n_p^{LS}\}$ and find the value λ_0 which minimizes $\sum F_j^2$. This is given by

$$\lambda_0^2 = C_0^2 \sum_{j=2}^{NC} \alpha_j \ln\left(\frac{E_j^{LS} g_1}{E_1^{LS} g_j}\right) \Big/ \sum_{j=2}^{NC} \alpha_j^2 \tag{13}$$

where

$$\alpha_j = \sum_{p=1}^{NP} \frac{n_p^{LS}}{\sigma_p^2}(S_{pj} - S_{p1})$$

and

$$C_0^2 = \sum_{p=1}^{NP} \left(n_p^{LS}\right)^2 \Big/ \sum_{p=1}^{NP} \sigma_p^2 .$$

The variance of this estimate can be large but it is useful in providing an initial value for λ if there are no other estimates available from previously computed solutions under similar conditions.

5. Additional points

The algorithm may have difficulty converging if the dynamic range in the values $\{g_c\}$ and $\{\sigma_p\}$ is too large. Care should be taken to ensure that $max\,(\{g_c\})/min\,(\{g_c\})$ and $max\,(\{\sigma_p\})/min\,(\{\sigma_p\})$ are within the numerical accuracy of the computations. Typically we do not use a dynamic range greater than 10^3. It is also sometimes necessary to compute a solution with a larger total noise than is desired and then continue the computation with a smaller requested noise value using the larger noise solution as a starting point.

D. Tests of the maximum entropy method

The algorithm was tested using the method described in section C. For comparison with the least squares method we used the same source and cell grid shown in Figs. 5 and 3 and the same input signals used to produce the least squares result in Fig. 4. For a default image we removed the asymmetrical component of the original source and took the square root of

the remaining profile. The default image is shown in Fig. 9. The standard deviations σ_p were all set equal to the standard deviation of the Gaussian noise generator. The result for $C = 0.95$ is shown in Fig. 10. The result for a flat default image is shown in Fig. 11.

Both maximum entropy cases are better than the unsmoothed least squares result. The maximum entropy result with a flat default image is slightly worse on average than the smoothed least squares result, but the accuracy in the central region is basically as good as the maximum entropy result using the better default image. The effect of the maximum entropy procedure is to pull the result towards the default image in the least well-determined regions. For the case of a flat default image, the effect in these regions is roughly equivalent to the smoothing applied to the least squares result.

An interesting example of the stability of the maximum entropy method is demonstrated by the reconstruction in Fig. 12. The default image is the same one used previously, see Fig. 9. The standard deviation used for each pixel was 3.5% of the signal with an overriding minimum standard deviation of 0.01% of the maximum signal. The corresponding unsmoothed least squares result is shown in Fig. 13. The original source is shown in Fig. 14. The erroneous structure on the inside edge of the bean is a series of ripples. See the 3D plot in Fig. 15. The 228 cell reconstruction grid is shown in Fig. 16. The errors in the least squares reconstruction occurred even though there was no noise in the original image supplied to the algorithm.

The main peculiarity of the original source is that it has a large gradient on the inside edge of the bean. The projection of the original source was computed using a slightly higher resolution grid than that used for the reconstruction. This 252 cell grid is shown in Fig. 17. The ripples in the least squares reconstruction can be shown to be due to the fact that the original source contains gradients which cannot be represented on the 228 cell grid used for the reconstruction. If we use the least squares method to reconstruct the image using the same 252 cell grid used for the projection, we get a perfect result as shown in Fig. 18. The maximum entropy method avoids the ripple error by allowing a larger RMS noise in the solution, 5.25% vs. 1.13% for the least squares result. This additional noise reflects the errors introduced by representing the source on the 228 cell grid.

E. Application to real data

The default image used for the reconstruction of real data is the set of magnetic flux surfaces produced by a MHD equilibrium fit to the external magnetic measurements of the plasma. The results of the reconstruction for two discharges are shown in figures 19 through 24. The reconstructions were done using the grid shown in Fig. 16. Figure 19 shows a reconstructed X-ray profile and Fig. 20 shows the flux surfaces used for the default image. Figure 21 shows a comparison between the actual camera image and the signal values obtained from the backprojection of the reconstruction.

The plot shows signal vs. camera pixel number for the actual and reconstructed image. The camera pixels are numbered 1 through 1024 and are scanned in 32 vertical columns of 32 pixels starting from the bottom right of the camera image.

Figure 22 shows the reconstructed X-ray profile for another discharge, Fig. 23 shows the default image, and Fig. 24 shows the comparison of actual and reconstructed data.

The RMS noise in these fits is quite high, but the reconstructed images are quite smooth. Examination of the comparison between the backprojected reconstructed image and the actual data seems to indicate that the deviations are caused by some type of systematic error. This could be caused by systematic errors in the camera data or in the mapping function or it could be a consequence of the finite resolution of the reconstruction grid if the source profile contains steep gradients. Further investigation will be necessary to determine the cause and possibly improve the fits.

IV. Conclusions

The maximum entropy algorithm has been implemented for an overdetermined system in a form which permits the computation of the result in a reasonable time on a VAX 8600. Comparison with the least squares algorithm shows that the maximum entropy is superior if a good default image can be constructed from additional information about the system. The algorithm permits the external magnetic information from MHD equilibrium fits to be combined with the X-ray pinhole camera data to produce an X-ray emission

profile which can be used to determine the internal magnetic structure of the plasma.

Acknowledgments

This work supported by the U.S. DOE fusion postdoctoral program administered by ORAU and U.S. DOE contract DE-AC02-76-CHO-3073.

Appendix

For the case of Poisson noise statistics, the equations in section III are replaced by the equations below.

$$P^{noise}(\{n_p\}|\{E_c\}) = \prod_{p=1}^{NP} \frac{a_p^{(I_p/\Delta I)} e^{-a_p}}{(I_p/\Delta I)!},$$

where ΔI is the quantum size of the signals $\{I_p\}$. Equation (7) is replaced by

$$F_j = \ln\left(\frac{E_j g_1}{E_1 g_j}\right) - \frac{\lambda^2}{C^2 \Delta I} \sum_{p=1}^{NP} \left(\frac{I_p}{a_p} - 1\right)(S_{pj} - S_{p1}) = 0, \quad j = 2 \rightarrow NC.$$

Equations (9) and (10) are replaced by

$$\frac{\partial F_j}{\partial E_j} = \frac{1}{E_1} + \frac{1}{E_j} + \frac{\lambda^2}{C^2 \Delta I} \sum_{p=1}^{NP} \frac{I_p}{a_p^2}(S_{pj} - S_{p1})^2, \quad j = 2 \rightarrow NC$$

and

$$\frac{\partial F_j}{\partial E_k} = \frac{1}{E_1} + \frac{\lambda^2}{C^2 \Delta I} \sum_{p=1}^{NP} \frac{I_p}{a_p^2}(S_{pj} - S_{p1})(S_{pk} - S_{p1}), \quad k \neq j \quad k, j = 2 \rightarrow NC.$$

Equation (11) remains the same except that $\sum \sigma_p^2$ is replaced by a suitable value for the expected total noise. Equation (12) is replaced with

$$F_j' = -\frac{2\lambda}{C^2 \Delta I} \sum_{p=1}^{NP} \frac{a_p}{a_p}(S_{pj} - S_{p1}).$$

Equation (13) remains the same with α_j given by

$$\alpha_j = \frac{1}{\Delta I} \sum_{p=1}^{NP} \left(\frac{I_p}{a_p} - 1 \right) (S_{pj} - S_{p1}).$$

References

[1]R. J. Fonck, M. Reusch, K. P. Jaehnig, R. Hulse, and P. Roney, "Soft X-ray imaging system for measurement of noncircular tokamak plasmas," *SPIE*, **691**, X-ray imaging II, 111 (1986).

[2]B. Roy Frieden, "Restoring with Maximum Likelihood and Maximum Entropy," J. Opt. Soc. Am. **62**, 511 (1972).

[3]A. Holland and G. A. Navratil, "Tomographic analysis of the evolution of plasma cross sections," Rev. Sci. Instrum. **57**, 1557 (1986).

[4]E. T. Powell, Ph.D. thesis Princeton University, 1990.

[5]R. Decoste, "X-ray tomography on plasmas with arbitrary cross sections and limited access," Rev. Sci. Instrum. **56**, 807 (1985).

[6]B. Roy Frieden, "Unified theory for estimating frequency-of-occurrence laws and optical objects," J. Opt. Soc. Am. **73**, 927 (1983).

[7]W. H. Press, B. P. Flannery, S. A. Teukolsky, W. T. Vettering, *Numerical Recipes*, p. 509 ff (Cambridge University Press, New York, 1986).

[8]B. Roy Frieden, D. C. Wells, "Restoring with maximum entropy. III. Poisson sources and backgrounds," J. Opt. Soc. Am. **68**, 93 (1978).

[9]E. S. Meinel, "Origins of linear and nonlinear recursive restoration algorithms," J. Opt. Soc. Am. A **3**, 787 (1986).

[10]E. S. Meinel, "Maximum-entropy image restoration: Lagrange and recursive techniques," J. Opt. Soc. Am. A **5**, 25 (1988).

[11]I. Barrodale, C. A. Zala, and R. F. MacKinnon, "Image processing by a maximum entropy procedure incorporating frequency domain bounds and prior knowledge," in *Conference Proceedings, IEEE Pacific Rim Conference on Communications, Computers and Signal Processing, June 4-5, 1987, Victoria, B.C.* (IEEE, New York, 1987).

[12]R. F. MacKinnon, "Minimum cross-entropy noise reduction in images," J. Opt. Soc. Am. A **6**, 739 (1989).

[13]W. H. Press, B. P. Flannery, S. A. Teukolsky, W. T. Vettering, *Numerical Recipes*, p. 254 ff (Cambridge University Press, New York, 1986).

Figures

FIG. 1. Pinhole camera's view of the plasma.

FIG. 2. Function showing relative contribution of each point in the source to the camera image.

FIG. 3. 130 cell grid used in reconstructions.

FIG. 4. Unsmoothed least squares reconstruction of source in Fig. 5. $\Delta_{rms} = 21.4\%$.

FIG. 5. Original source for tests.

FIG. 6. Least squares reconstruction with one smoothing pass. $\Delta_{rms} = 16.6\%$.

FIG. 7. 76 cell grid used in reconstructions.

FIG. 8. Unsmoothed least squares reconstruction using 76 cell grid. $\Delta_{rms} = 12.9\%$.

FIG. 9. Default image used for maximum entropy reconstruction tests. $\Delta_{rms} = 42.7\%$.

FIG. 10. Maximum entropy reconstruction using bean-shaped default image. $\Delta_{rms} = 10.8\%$.

FIG. 11. Maximum entropy reconstruction using flat default image. $\Delta_{rms} = 18.1\%$.

FIG. 12. Maximum entropy reconstruction of source in Fig. 14 using default image in Fig. 9 and 228 cell grid in Fig. 16. $\Delta_{rms} = 10\%$.

FIG. 13. Unsmoothed least squares reconstruction of source in Fig. 14 using 228 cell grid. $\Delta_{rms} = 20.7\%$.

FIG. 14. Source used to demonstrate errors caused by large gradients.

FIG. 15. 3D plot of result in Fig. 13.

FIG. 16. 228 cell grid used for reconstruction of source in Fig. 14.

FIG. 17. 252 cell grid used to specify source in Fig. 14.

FIG. 18. Unsmoothed least squares reconstruction of source in Fig. 14 using 252 cell grid. $\Delta_{rms} = 0\%$.

FIG. 19. Maximum entropy reconstruction of a real plasma source using the default image in Fig. 20. $\Delta_{rms} = 16.9\%$.

FIG. 20. Equilibrium magnetic flux surfaces used as a default image for the reconstruction in Fig. 19.

FIG. 21. Comparison of the signals on each pixel in the camera image produced by the real data and the backprojection of the reconstructed X-ray profile for the reconstruction in Fig. 19.

FIG. 22. Maximum entropy reconstruction of another discharge using the default image in Fig. 23. $\Delta_{rms} = 27.7\%$.

FIG. 23. Equilibrium magnetic flux surfaces used as a default image for the reconstruction in Fig. 22.

FIG. 24. Comparison of the signals on each pixel in the camera image produced by the real data and the backprojection of the reconstructed X-ray profile for the reconstruction in Fig. 22.

PBX-M SOFT X-RAY CAMERA.

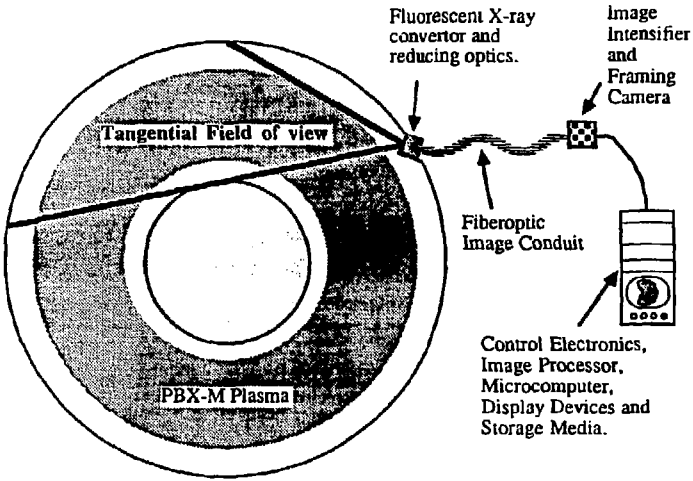

Figure 1

Detector configuration for datafile MFOP.R

1024 active channels 0 deleted channels

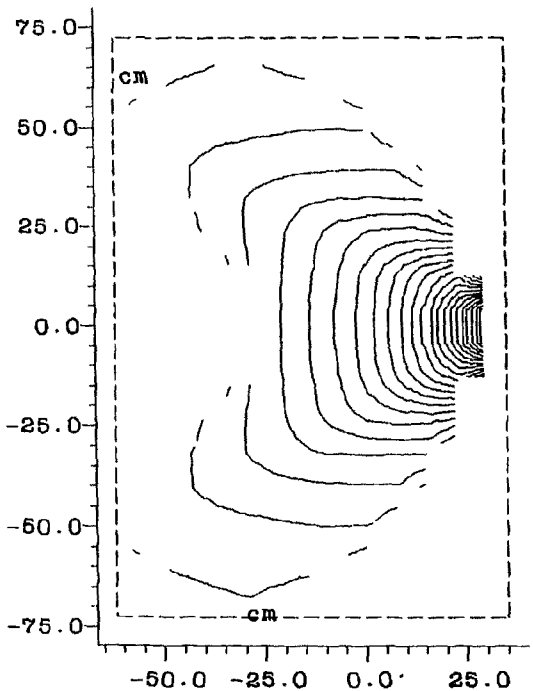

Figure 2

Weight file name
MFOP.R
Matrix origin
R = -80.28 cm
Z = -67.97 cm
Cell size
R = 7.438 cm
Z = 9.063 cm
152 Normal cells
0 Odd cells
152 Matrix cells

Weight contour levels
Level 1 = 4.295E-05
Increment = 2.075E-04
Weight range
Minimum = 7.266E-13
Maximum = 8.760E-05

Detector configuration for datafile MS3P_newfmt.R

1024 active channels 0 deleted channels

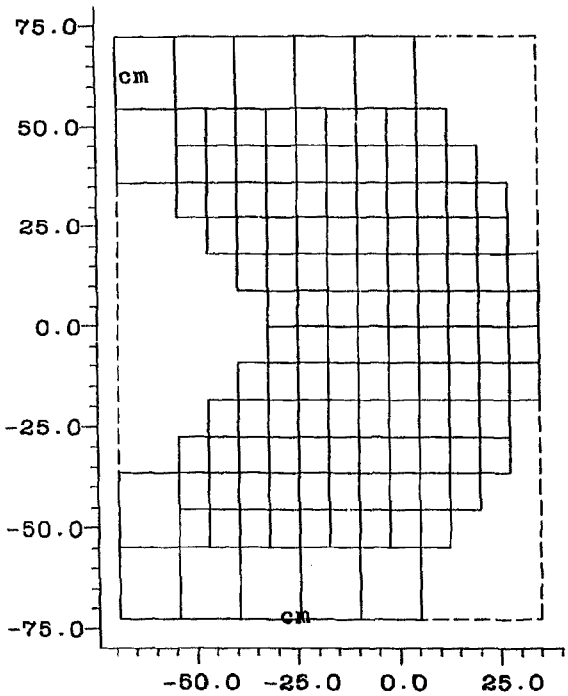

Figure 3

Weight file name
MS3P_newfmt.R
Matrix origin
R = -80.28 cm
Z = -67.97 cm
Cell size
R = 7.438 cm
Z = 9.063 cm
130 Normal cells
0 Odd cells
-1 Matrix cells

Reconstructed numerical phantom. File :- 3MS3P.E

1024 active channels

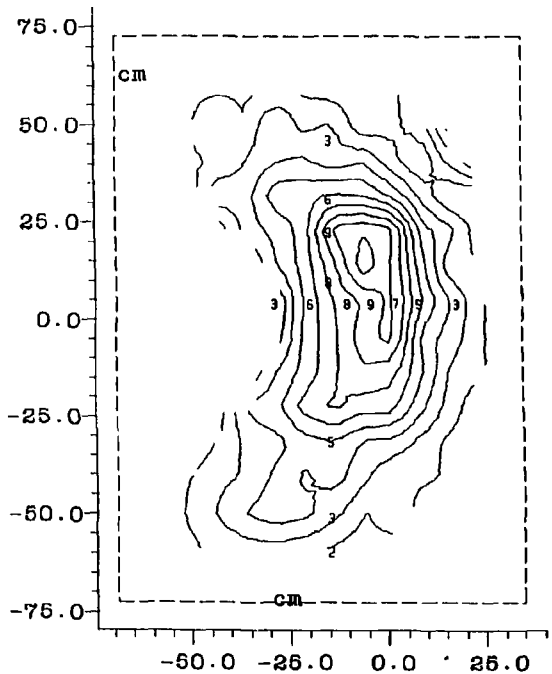

RMS reconstruction error 21.4 %
RMS resolution error 0.000E+00 %
Average error 1.32 %
RMS shape error 21.3 %
Simulated rms projection error 10.0 %
Actual rms projection error 9.93 %
Simulated noise type = 1
Gaussian simulated noise.
Number of random number cycles = 0
Processing Linear
Emission contour levels
Level 1 = 0.000E+00
Increment = 0.100
Emission range
Minimum = 0.000E+00
Maximum = 0.965
Average = 0.286203
RMS noise = 9.43 %
Blind noise = 6.18 %
Number of cells = 130
Reconstruction time = 0.000E+00 s.
Matrix inversion algorithm.
Datafile MS3P.R

Reconstruction using matrix inversion.
Number of emissions <= 0.0 was 12
Emissions <= 0.0 set to 0.000E+00 % average.
Weight file MS3P.R
Matrix origin
R = -80.281 cm
Z = -67.969 cm
Cell size
R = 7.438 cm
Z = 9.063 cm

Figure 4

Best possible phantom reconstruction. File :- 3MS3P.E

1024 active channels

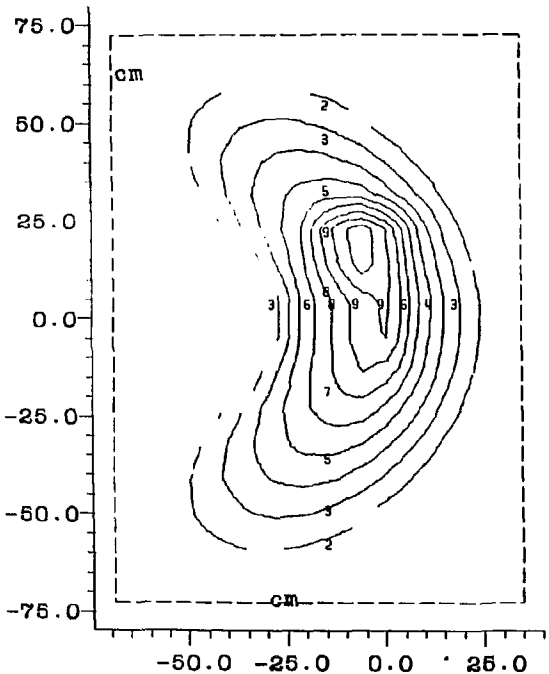

RMS reconstruction error 0.000E+00 %
RMS resolution error 0.000E+00 %
Average error 1.32 %
RMS shape error 16.6 %
Processing Linear
Emission contour levels
Level 1 = 0.000E+00
Increment = 0.100
Emission range
Minimum = 1.382E-04
Maximum = 0.977
Average = 0.266203

Datafile MS3P.R

Reconstruction using matrix inversion.
Number of emissions <= 0.0 was 12
Emissions <= 0.0 set to 0.000E+00 % average.
Number of bilinear smoothing passes = 1
Weight file MS3P.R
Matrix origin
R = -60.281 cm
Z = -67.969 cm
Cell size
R = 7.438 cm
Z = 9.063 cm

Reconstructed numerical phantom. File :- 3MS3P.E

1024 active channels

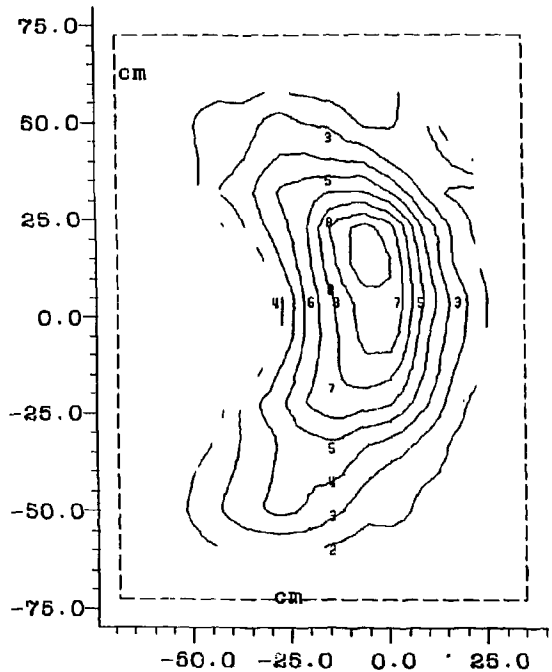

RMS reconstruction error 16.6 %
RMS resolution error 0.000E+00 %
Average error 1.32 %
RMS shape error 16.6 %
Simulated rms projection error 10.0 %
Actual rms projection error 9.93 %
Simulated noise type - 1
Gaussian simulated noise.
Number of random number cycles - 0
Processing Linear
Emission contour levels
Leve 1 - 0.000E+00
Increment - 0.100
Emission range
Minimum - 0.000E+00
Maximum - 0.894
Average - 0.266203
RMS noise - 10.4 %
Blind noise - 4.30 %
Number of cells - 130
Reconstruction time - 0.000E+00 s.
Matrix inversion algorithm.
Datafile MS3P.R

Reconstruction using matrix inversion.
Number of emissions <= 0.0 was 12
Emissions <= 0.0 set to 0.000E+00 % average.
Number of bilinear smoothing passes - 1
Weight file MS3P.R
Matrix origin
R - -80.281 cm
Z - -67.969 cm
Cell size
R - 7.438 cm
Z - 9.063 cm

Figure 6

Detector configuration for datafile MS2P.R

1024 active channels 0 deleted channels

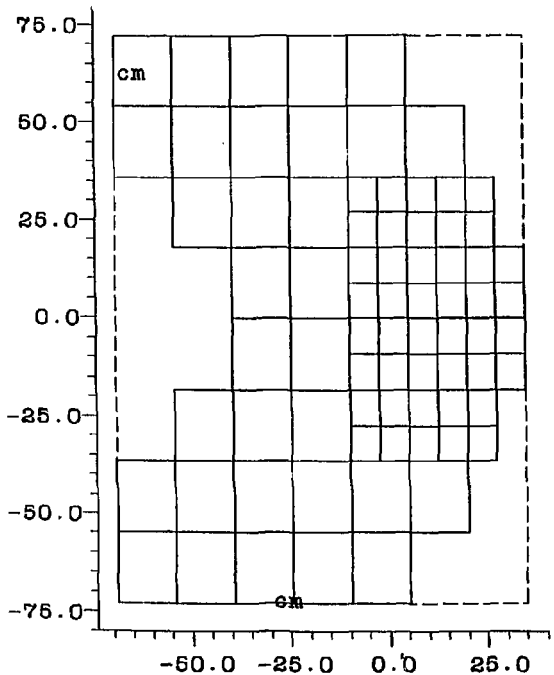

Figure 7

Weight file name
MS2P.R
Matrix origin
R = -80.28 cm
Z = -68.38 cm
Cell size
R = 7.438 cm
Z = 9.063 cm
76 Normal cells
0 Odd cells
-1 Matrix cells

Reconstructed numerical phantom. File :- 3MS3P.E

1024 active channels

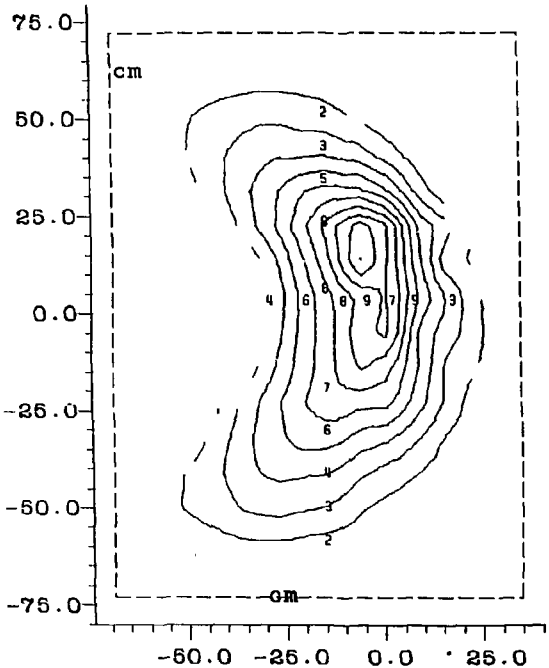

RMS reconstruction error 12.9 %
RMS resolution error 0.000E+00 %
Average error 1.14 %
RMS shape error 12.8 %
Simulated rms projection error 10.0 %
Actual rms projection error 9.83 %
Simulated noise type = 1
Gaussian simulated noise.
Number of random number cycles = 0
Processing Linear
Emission contour levels
Level 1 = 0.000E+00
Increment = 0.100
Emission range
Minimum = 0.000E+00
Maximum = 1.01
Average = 0.287413
RMS noise = 10.7 %
Blind noise = 4.06 %
Number of cells = 76
Reconstruction time = 0.000E+00 s.
Matrix inversion algorithm.
Datafile MS3P.R

Reconstruction using matrix inversion.
Number of emissions <= 0.0 was 8
Emissions <= 0.0 set to 0.000E+00 % average.
Weight file MS2P.R
Matrix origin
R = -80.281 cm
Z = -88.375 cm
Cell size
R = 7.438 cm
Z = 9.083 cm

Figure 8

Distorted a priori estimate of phantom. File :- 3MS3P.E

1024 active channels

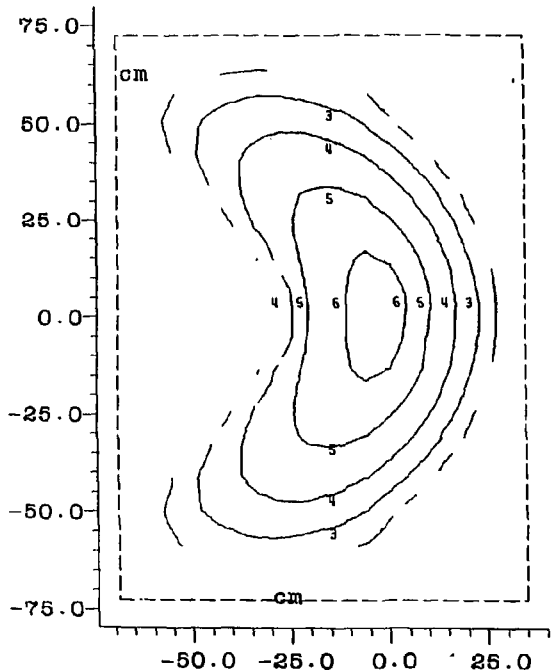

RMS reconstruction error 42.7 %
RMS resolution error 0.000E+00 %
Average error 0.000E+00 %
RMS shape error 40.8 %
Processing Linear
Emission contour levels
Level 1 = 0.000E+00
Increment = 0.100
Emission range
Minimum = 1.085E-03
Maximum = 0.555
Average = 0.262691

Datafile MS3P.R

Default image file 3MF3P.D
Weight file MS3P.R
Matrix origin
R = -80.281 cm
Z = -67.969 cm
Cell size
R = 7.438 cm
Z = 9.063 cm

Figure 9

Reconstructed numerical phantom. File :- 3MS3P.E

1024 active channels

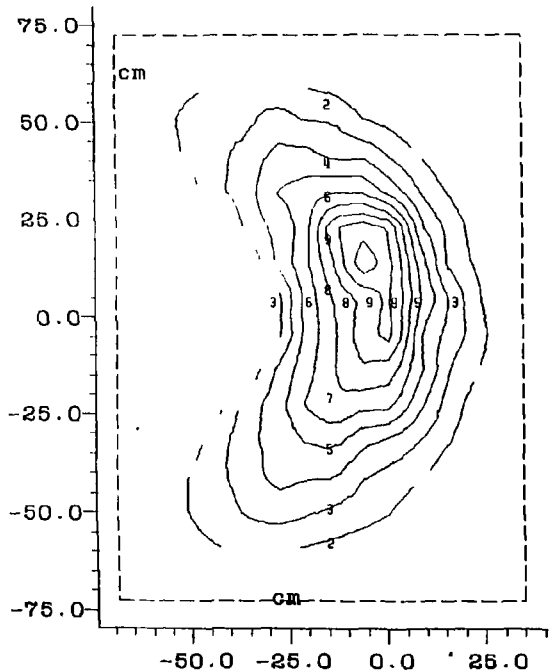

RMS reconstruction error 10.8 %
RMS resolution error 0.000E+00 %
Average error 1.32 %
RMS shape error 10.8 %
Simulated rms projection error 10.0 %
Actual rms projection error 9.93 %
Simulated noise type = 1
Gaussian simulated noise.
Number of random number cycles = 0
Processing Linear
Emission contour levels
Level 1 = 0.000E+00
Increment = 0.100
Emission range
Minimum = 3.799E-04
Maximum = 0.980
Average = 0.266203
Gaussian noise statistics.
Noise level = 0.950
Sharpness = 1.143E+09
RMS Std. dev. = 9.99 %
Std. dev. type = 0
RMS noise = 9.49 %
Blind noise = 5.11 %
Number of cells = 130
Number of iterations = 8
Reconstruction time = 41.2 s.
Fast ME algorithm.
Datafile MS3P.R

Default image file 3MF3P.D
Weight file MS3P.R
Matrix origin
R = -80.281 cm
Z = -67.969 cm
Cell size
R = 7.438 cm
Z = 9.083 cm

Figure 19

Reconstructed numerical phantom. File :- 3MS3P.E

1024 active channels

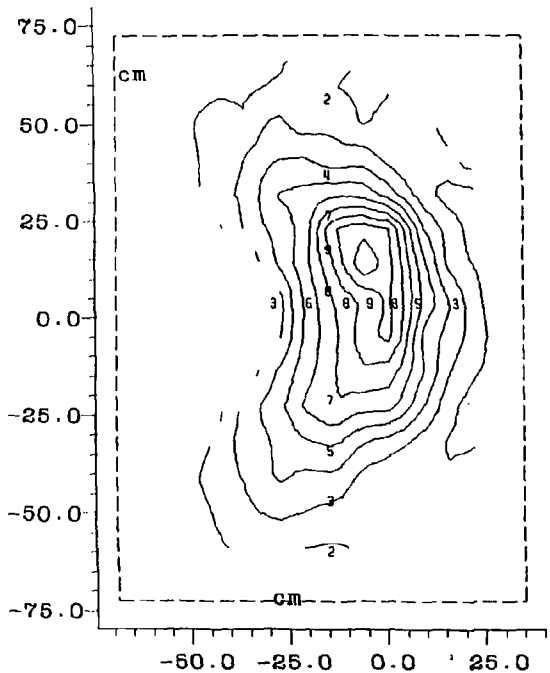

RMS reconstruction error 18.1 %
RMS resolution error 0.000E+00 %
Average error 1.32 %
RMS shape error 18.1 %
Simulated rms projection error 10.0 %
Actual rms projection error 9.93 %
Simulated noise type - 1
Gaussian simulated noise.
Number of random number cycles - 0
Processing Linear
Emission contour levels
Level 1 - 0.000E+00
Increment - 0.100
Emission range
Minimum - 7.557E-04
Maximum - 0.967
Average - 0.266203
Gaussian noise statistics.
Noise level - 0.950
Sharpness - 2.828E+09
RMS Std. dev. - 9.99 %
Std. dev. type - 0
RMS noise - 9.50 %
Blind noise - 5.10 %
Number of cells - 130
Number of iterations - 9
Reconstruction time - 35.4 s.
Fast ME algorithm.
Datafile MS3P.R

Default image is flat.
Weight file MS3P.R
Matrix origin
R - -80.281 cm
Z - -67.969 cm
Cell size
R - 7.438 cm
Z - 9.063 cm

Reconstructed numerical phantom. File :- EDBEAN5P4R.E

1024 active channels

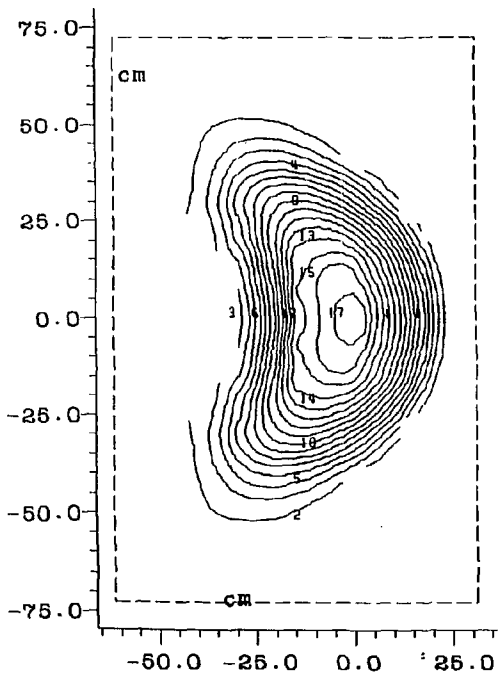

RMS reconstruction error 10.0 %
RMS resolution error 0.000E+00 %
Average error 0.528 %
RMS shape error 9.55 %
Simulated rms projection error 0.000E+00 %
Actual rms projection error 0.000E+00 %
Simulated noise type = 0
Uniform simulated noise.
Number of random number cycles = 0
Processing Linear
Emission contour levels
Level 1 = 0.000E+00
Increment = 15.0
Emission range
Minimum = 3.451E-12
Maximum = 253.
Average = 83.4901
Gaussian noise statistics.
Noise level = 0.350
Sharpness = 8.710E+06
RMS Std. dev. = 15.0 %
Std. dev. type = 1
Std. dev. min = 2.000E-05
Std. dev. min = 4.236E-02 % of max signal.
Std. dev. = 0.000E+00 % of signal.
RMS noise = 5.25 %
Blind noise = 0.000E+00 %
Number of cells = 228
Number of iterations = 62
Reconstruction time = 62.0 s.
Fast ME algorithm.
Datafile MF4P.R

Default image file 3MF4P.D
Weight file MF4P.R
Matrix origin
R = -82.141 cm
Z = -70.234 cm
Cell size
R = 3.719 cm
Z = 4.531 cm

Figure 12

Reconstructed numerical phantom. File :- EDBEAN5P4R.E

1024 active channels

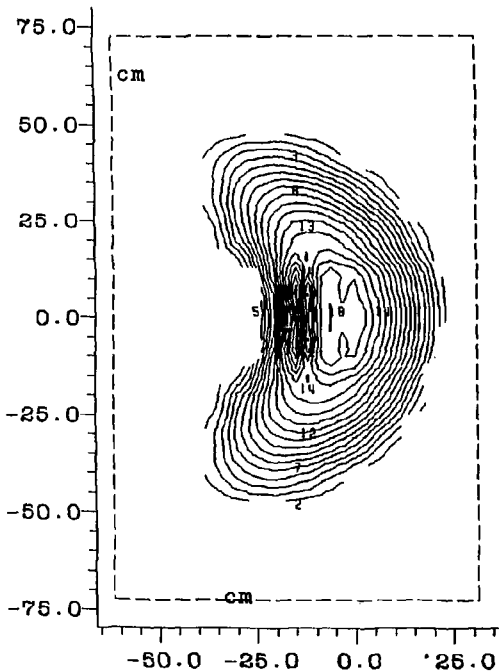

RMS reconstruction error 20.7 %
RMS resolution error 0.000E+00 %
Average error 0.528 %
RMS shape error 20.4 %
Simulated rms projection error 0.000E+00 %
Actual rms projection error 0.000E+00 %
Simulated noise type = 0
Uniform simulated noise.
Number of random number cycles = 0
Processing Linear
Emission contour levels
Level 1 = 0.000E+00
Increment = 15.0
Emission range
Minimum = 0.000E+00
Maximum = 295.
Average = 83.4901
RMS noise = 1.13 %
Blind noise = 0.000E+00 %
Number of cells = 228
Reconstruction time = 23.9 s.
Matrix inversion algorithm.
Datafile HF4P.R

Reconstruction using matrix inversion.
Number of emissions <= 0.0 was 52
Emissions <= 0.0 set to 0.000E+00 % average.
Weight file HF4P.R
Matrix origin
R = -82.141 cm
Z = -70.234 cm
Cell size
R = 3.719 cm
Z = 4.531 cm

Distorted a priori estimate of phantom. File :-

1024 active channels

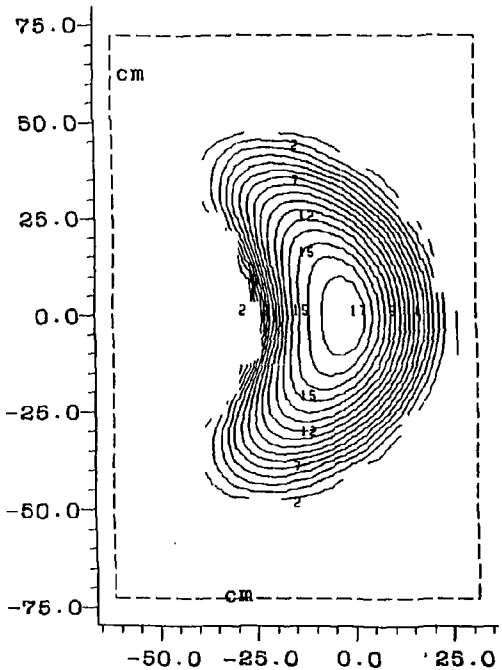

Time 5.500 msec
Processing Linear
Emission contour levels
Level 1 = 0.000E+00
Inorement = 15.0
Emission range
Minimum = 0.000E+00
Maximum = 254.
Average = 0.000000E+00

Datafile MF5P.R

Default image file EDBEAN5P.D
Weight file MF6P.R
Matrix origin
R = -82.141 cm
Z = -70.234 cm
Cell size
R = 3.719 cm
Z = 4.531 cm

Figure 14

PBX Soft X-ray Emission Cross-section. Shot # 0

1024 active channels

Time 0.000 msec Minimum emission= 0.000E+00 Maximum emission= 295. Average= 83.4901
Processing Linear Datafile MF4P.R Weight file MF4P.R
Reconstruction using matrix inversion. Emissions <= 0.0 set to 0.000E+00 % average.
Number of emissions <= 0.0 was 52
Matrix origin R = -82.141 cm Z = -70.234 cm Cell size R = 3.719 cm Z = 4.531 cm

RMS noise = 1.13 % Blind noise = 0.000E+00 % Std. dev. type = 1
Number of cells = 228 Number of iterations = 81 Reconstruction time = 23.9 s. Matrix inversion algorithm.

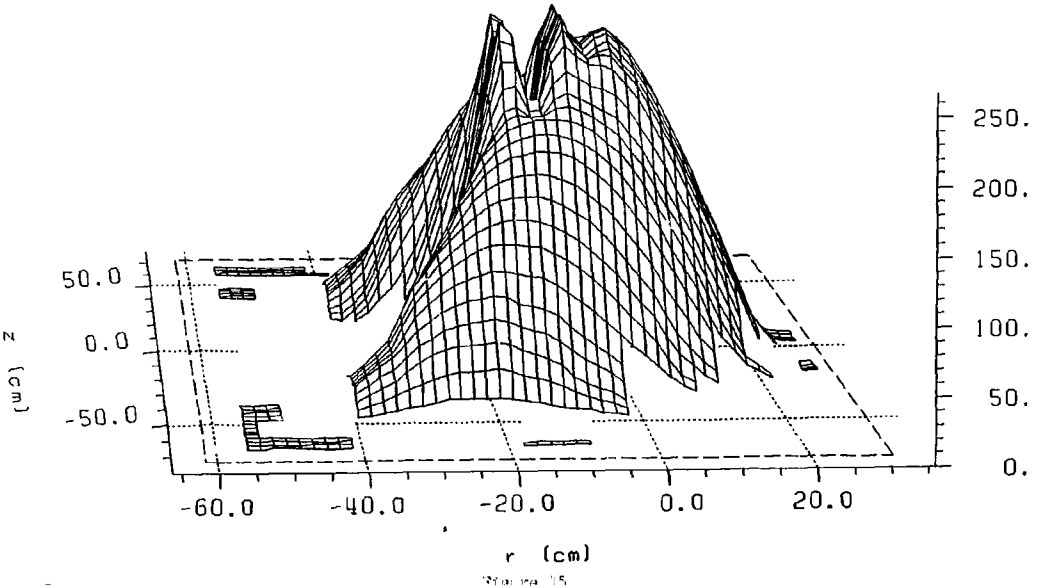

Detector configuration for datafile MF4P.R

1024 active channels 0 deleted channels

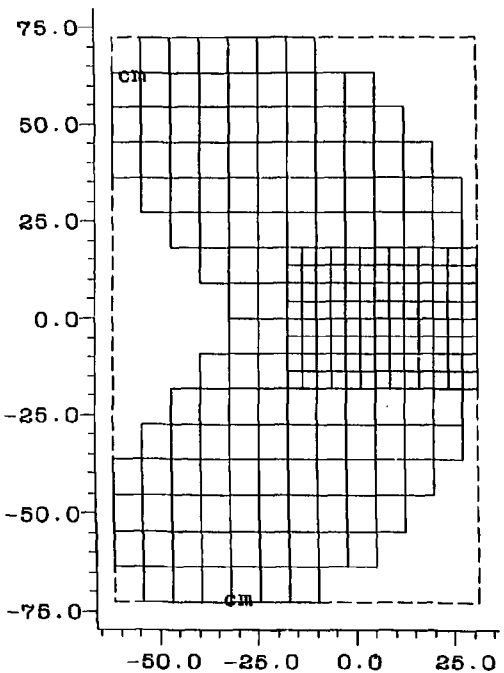

Weight file name
MF4P.R
Matrix origin
R = -82.14 cm
Z = -70.23 cm
Cell size
R = 3.719 cm
Z = 4.631 cm
228 Normal cells
0 Odd cells
-1 Matrix cells

Figure 16

Detector configuration for datafile MF5P.R

1024 active channels 0 deleted channels

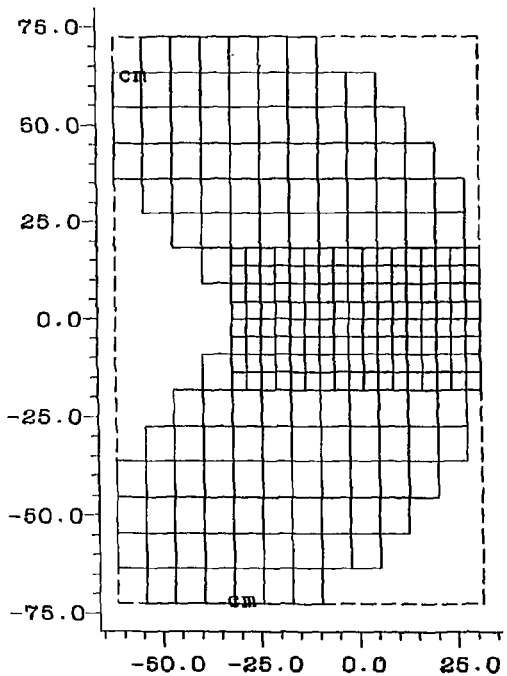

Weight file name
MF5P.R
Matrix origin
R = -82.14 cm
Z = -70.23 cm
Cell size
R = 3.719 cm
Z = 4.631 cm
252 Normal cells
0 Odd cells
-1 Matrix cells

Reconstructed numerical phantom. File :- EDBEAN5P4R.E

1024 active channels

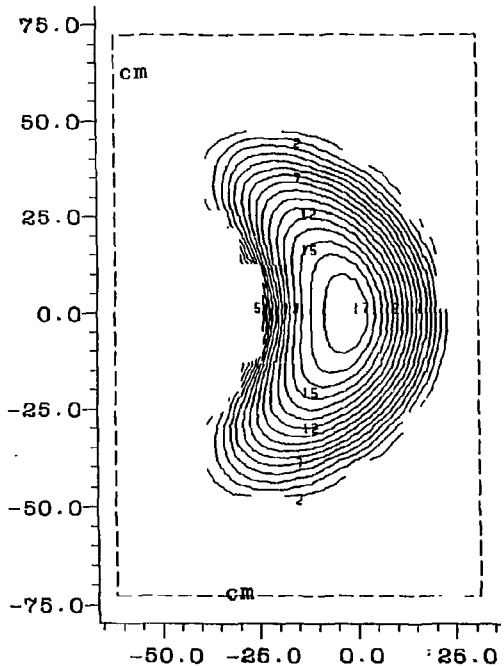

RMS reconstruction error 0.000E+00 %
RMS resolution error 0.000E+00 %
Average error 7.153E-05 %
RMS shape error 0.000E+00 %
Simulated rms projection error 0.000E+00 %
Actual rms projection error 0.000E+00 %
Simulated noise type = 0
Uniform simulated noise.
Number of random number cycles = 0
Processing Linear
Emission contour levels
Level 1 = 0.000E+00
Increment = 15.0
Emission range
Minimum = 0.000E+00
Maximum = 254.
Average = 82.3024
RMS noise = 1.682E-04 %
Blind noise = 0.000E+00 %
Number of cells = 252
Reconstruction time = 0.000E+00 s.
Matrix inversion algorithm.
Datafile MF4P.R

Reconstruction using matrix inversion.
Number of emissions <= 0.0 was 66
Emissions <= 0.0 set to 0.000E+00 % average.
Weight file MF5PDP.R
Matrix origin
R = -82.141 cm
Z = -70.234 cm
Cell size
R = 3.719 cm
Z = 4.531 cm

Figure 18

PBX Soft X-ray Emission Cross-section. Shot # 269084

1024 active channels

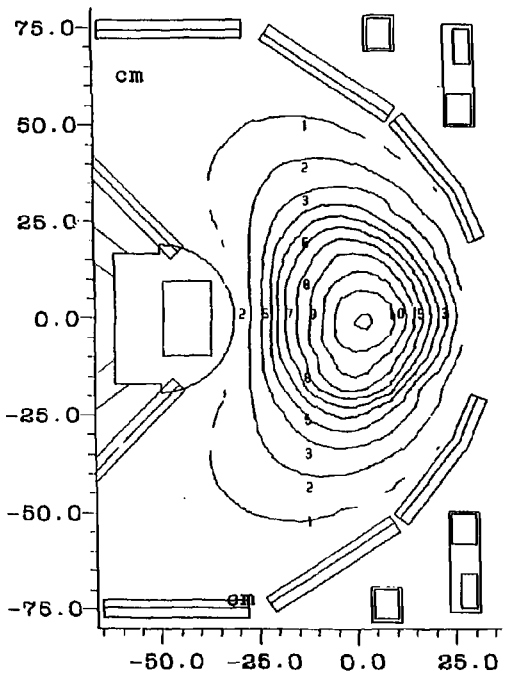

Time 430.000 msec
Processing Linear
Emission contour levels
Level 1 = 1.000E+05
Increment = 4.000E+05
Emission range
Minimum = 912.
Maximum = 4.212E+06
Average = 1.246575E+06
Gaussian noise statistics.
Noise level = 1.00
Sharpness = 26.0
RMS Std. dev. = 4.51 %
Std. dev. type = 0
RMS noise = 18.9 %
Blind noise = 4.81 %
Number of cells = 218
Number of iterations = 12
Reconstruction time = 12.0 s.
Fast ME algorithm.
Datafile CNTR_PERP.LATE

Default image file W:269084_430Q070.D
Weight file MF4R.R
Matrix origin
R = -67.000 cm
Z = 66.000 cm
Cell size
R = 4.000 cm
Z = 4.000 cm

Figure 19

Distorted a priori estimate of phantom. File :-

1024 active channels

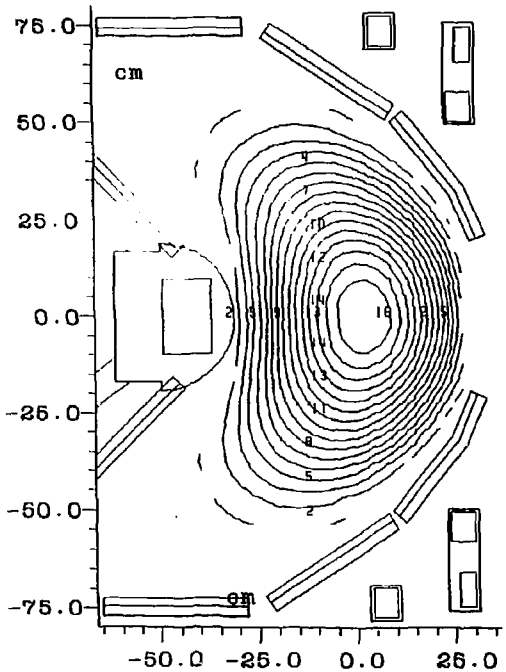

Time 5.500 msec
Processing Linear
Emission contour levels
Level 1 - 500.
Increment - 2.000E+03
Emission range
Minimum - 11.8
Maximum - 3.264E+04
Average - 0.000000E+00

Datafile

Default image file W:269084_430Q070.D
Weight file MF4R.R
Matrix origin
R - -67.000 cm
Z - 66.000 cm
Cell size
R - 4.000 cm
Z - 4.000 cm

Figure 20

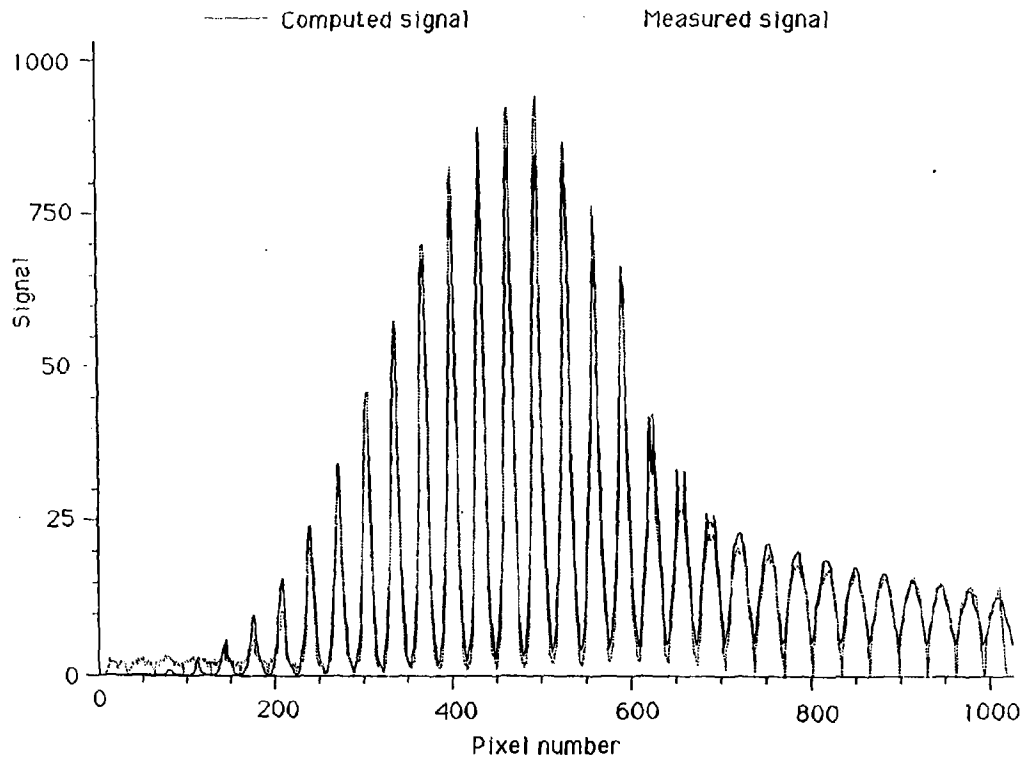
Computed signal
Measured signal
1000
750
50
25
0
Signal
0
200
400
600
800
1000
Pixel number

Figure 21

PBX Soft X-ray Emission Cross-section. Shot # 260501

1024 active channels

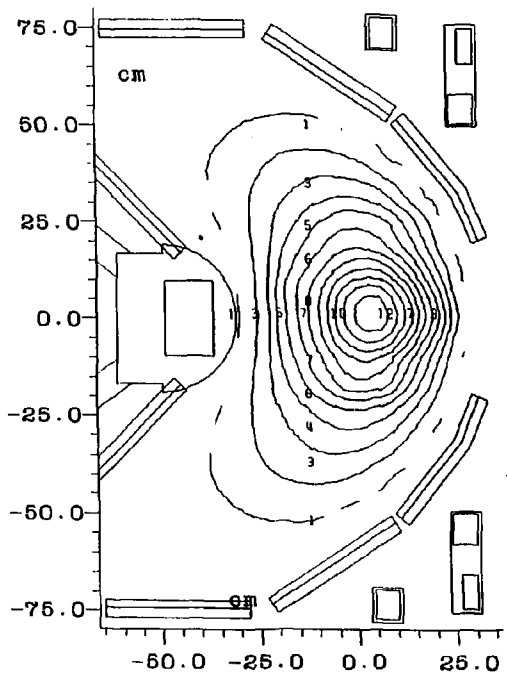

Time 520.000 msec
Processing Linear
Emission contour levels
Level 1 = 1.000E+05
Increment = 4.000E+05
Emission range
Minimum = 802.
Maximum = 4.833E+06
Average = 1.206690E+06
Gaussian noise statistics.
Noise level = 2.00
Sharpness = 14.8
RMS Std. dev. = 4.89 %
Std. dev. type = 0
RMS noise = 27.7 %
Blind noise = 0.590 %
Number of cells = 218
Number of iterations = 9
Reconstruction time = 61.9 s.
Fast ME algorithm.
Datafile CO_PARA2.LATE

Default image file W:260501_520Q040.D
Weight file HF4R.R
Matrix origin
R = -67.000 cm
Z = -66.000 cm
Cell size
R = 4.000 cm
Z = 4.000 cm

Figure 22

Distorted a priori estimate of phantom. File :-

1024 active channels

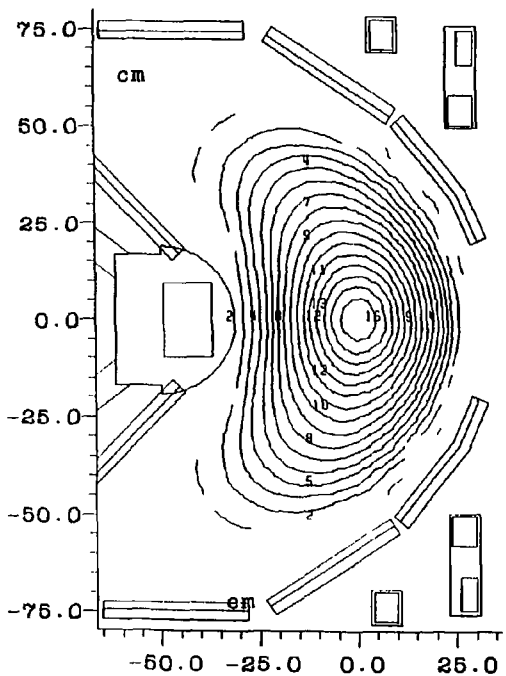

Time 440.000 msec
Processing Linear
Emission contour levels
Level 1 - 500.
Increment - 2.000E+03
Emission range
Minimum - 9.74
Maximum - 3.241E+04
Average - 782608.

Datafile CNTR_PARA.LATE

Default image file W:260501_520Q040
Weight file MF4R.R
Matrix origin
R - -67.000 cm
Z - -66.000 cm
Cell size
R - 4.000 cm
Z - 4.000 cm

Figure 23

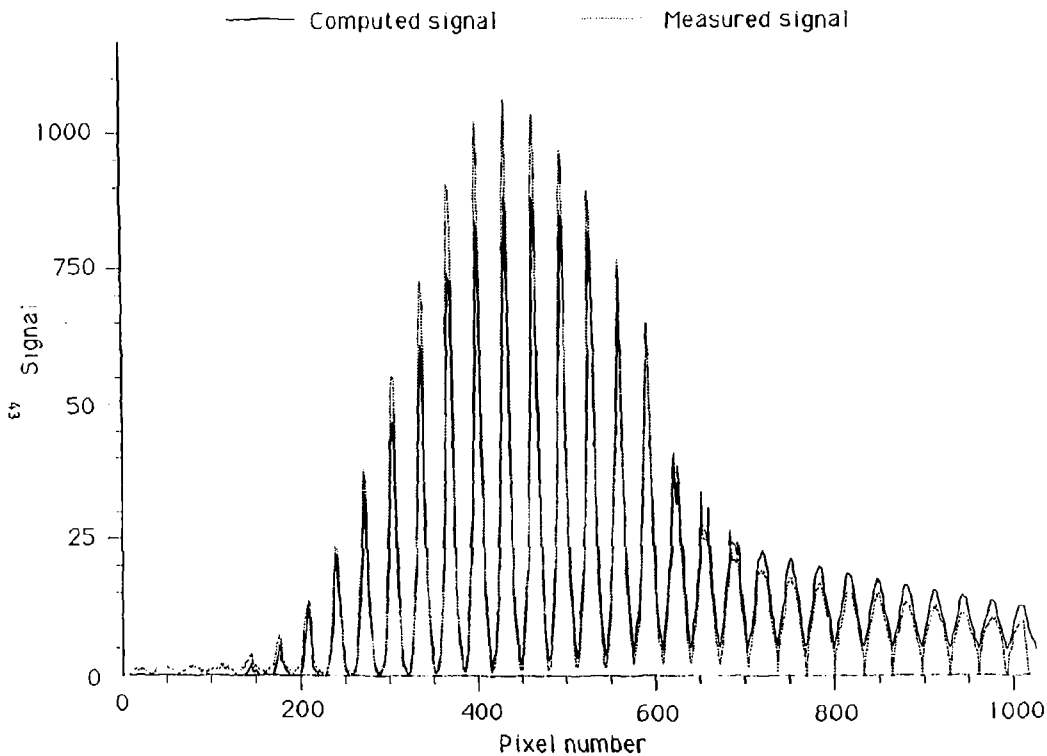
Computed signal
Measured signal
1000
750
50
25
0
Signal
0
200
400
600
800
1000
Pixel number

Figure 24

NOTICE

Available from:

National Technical Information Service
U.S. Department of Commerce
5285 Port Royal Road
Springfield, Virginia 22161
703-487-4650

Use the following price codes when ordering:

Price: Printed Copy A03
Microfiche A01

DISCLAIMER

This report was prepared as an account of work sponsored by an agency of the United States Government. Neither the United States Government nor any agency thereof, nor any of their employees, makes any warranty, express or implied, or assumes any legal liability or responsibility for the accuracy, completeness, or usefulness of any information, apparatus, product, or process disclosed, or represents that its use would not infringe privately owned rights. Reference herein to any specific commercial product, process, or service by trade name, trademark, manufacturer, or otherwise does not necessarily constitute or imply its endorsement, recommendation, or favoring by the United States Government or any agency thereof. The views and opinions of authors expressed herein do not necessarily state or reflect those of the United States Government or any agency thereof.